

Two New Hydrated Oxyhydroxides $\text{Sr}_3\text{Co}_{1.7}\text{Ti}_{0.3}\text{O}_5(\text{OH})_{2,x}\text{H}_2\text{O}$ and $\text{Sr}_4\text{Co}_{1.6}\text{Ti}_{1.4}\text{O}_8(\text{OH})_{2,x}\text{H}_2\text{O}$ Derived from the RP $n = 2$ and 3 Members: Structural and Magnetic Behavior versus Temperature

D. Pelloquin,* N. Barrier, D. Flahaut, V. Caignaert, and A. Maignan

Laboratoire CRISMAT, UMR 6508 CNRS ENSICAEN, 6 bd Maréchal Juin, 14050 CAEN Cedex 4 France

Received September 9, 2004

By varying the cobalt/titanium ratio, two hydrated oxyhydroxides have been prepared in air. The structural study by transmission electron microscopy techniques and thermal analyses shows that these compounds, $\text{Sr}_3\text{Co}_{1.7}\text{Ti}_{0.3}\text{O}_5(\text{OH})_{2,x}\text{H}_2\text{O}$ and $\text{Sr}_4\text{Co}_{1.6}\text{Ti}_{1.4}\text{O}_8(\text{OH})_{2,x}\text{H}_2\text{O}$ are derived from the Ruddlesden–Popper $n = 2$ and 3 members, respectively. The temperature dependence of the structure shows upon a broad structural transition being warmed from hydrated to anhydrous oxyhydroxides. In the last form, the cobalt/titanium cations adopt a square pyramidal coordination with a long (Co/Ti)–OH apical distance. The phenomenon of water loss during being warmed to 200 °C to obtain these oxyhydroxides is found to be reversible. The magnetic behavior of these phases is governed by the substituted amount of Ti^{4+} (d^0) for cobalt species: cluster- and spin-glass-like properties are observed for the hydrated oxyhydroxides derived from the RP $n = 2$ and 3 members, respectively.

Introduction

The recent discovery of a large thermoelectric power in the metallic phase NaCo_2O_4 ¹ and of superconductivity ($T_c = 4.5$ K) for the derived hydrated compound $\text{Na}_{0.3}\text{CoO}_2 \cdot (\text{H}_2\text{O})_{1.3}$ ² shows that the search for new layered hydrated cobaltites is important. The layered Ruddlesden – Popper (RP) type phases, first stabilized for titanium with the $\text{Sr}_{n+1}\text{Ti}_n\text{O}_{3n+1}$ formula,³ provide a very promising series in which the thickness of the perovskite blocks, sandwiched between the $[\text{SrO}]_\infty$ NaCl-type layers, allows one to play with the dimensionality of the properties. Furthermore, the choice of this series is also motivated by the recent discovery of an iron based layered oxide intercalating water molecules in which the mother framework, $\text{Sr}_3\text{NdFe}_3\text{O}_{8.5+\delta}$, is an oxygen deficient $n = 3$ RP member.⁴ Interestingly, this RP member reacts with ambient moisture to transform into a hydrated oxyhydroxide $\text{Sr}_3\text{NdFe}_3\text{O}_{7.5}(\text{OH})_{2,x}\text{H}_2\text{O}$.⁴ This suggests that several hydrated oxyhydroxides $\text{Sr}_{n+1}\text{MT}_n\text{O}_{3n+1}(\text{OH})_{2,x}\text{H}_2\text{O}$, where MT is a transition metal, can be stabilized. The structural mechanism describing the formation of the latter (Figure 1) consists of a topotactic hydrolysis/hydration reaction of the mother $\text{Sr}_{n+1}\text{MT}_n\text{O}_{3n+1}$ RP members. The major structural change consists of the insertion at the level of the rocksalt-type layer of two (OH^-) groups and an H_2O molecule. Consequently, the thickness of this layer block, separating two successive blocks of perovskite layers, is increased by about 6.2 Å. Then, by removing the intercalated

H_2O molecule, one obtains the $\text{Sr}_{n+1}\text{MT}_n\text{O}_{3n+1}(\text{OH})_2$ oxyhydroxide for which the thickness of the separating block, about 4.6 Å, is intermediate between those of the corresponding starting RP phases (about 2.7 Å) and the hydrated oxyhydroxide (Figure 1).

Keeping in mind this structural mechanism, the cobalt based Ruddlesden–Popper series has been chosen as a starting material since the existence of a large oxygen nonstoichiometry reported in the $n = 2$ RP member $\text{Sr}_3\text{Co}_2\text{O}_{6\pm\delta}$ ⁵ could favor the introduction of (OH^-) groups. In the following paper, we report on the discovery of two new air-hydrated oxyhydroxides, $\text{Sr}_3\text{Co}_{1.7}\text{Ti}_{0.3}\text{O}_5(\text{OH})_{2,x}\text{H}_2\text{O}$ and $\text{Sr}_4\text{Co}_{1.6}\text{Ti}_{1.4}\text{O}_8(\text{OH})_{2,x}\text{H}_2\text{O}$, in which structures are derived from the $n = 2$ and 3 RP members, respectively. In these phases, the Ti/Co ratio is found to control the thickness of the perovskite block but also the strength of the magnetic interactions. The dehydration at low temperature ($T \approx 200$ °C) of these phases demonstrates that these (Co/Ti) hydrated oxyhydroxides are good candidates for the process of water intercalation/deintercalation. In addition, in the intermediate temperature range, ~ 200 °C, the structure study shows that two new oxyhydroxides can be stabilized with the following formulas, $\text{Sr}_3\text{Co}_{1.7}\text{Ti}_{0.3}\text{O}_5(\text{OH})_2$ and $\text{Sr}_4\text{Co}_{1.6}\text{Ti}_{1.4}\text{O}_8(\text{OH})_2$.

Experimental Procedures

The samples were prepared in air by using powders of SrCO_3 (99.5%), Co_3O_4 (99%), and TiO_2 (99%). These precursors were weighted in stoichiometric proportions, intimately ground in an agate mortar, and pressed in the form of bars. The bars, set in an alumina vessel, were fired for 5 days at 1275 °C and then quenched in air. The products were poorly sintered black bars, and they were found to become powders at room temperature after exposure in air for ~ 12 h.

* Corresponding author. E-mail: denis.pelloquin@ismra.fr.

- (1) Terasaki, I.; Sasago, Y.; Uchinokura, K. *Phys. Rev. B* **1997**, *56*, R12685.
- (2) Takada, K.; Sakurai, H.; Takayama-Muromachi, E.; Izumi, F.; Dilanian, R. A.; Sasaki, T. *Nature* **2003**, *422*, 53.
- (3) Ruddlesden, S. N.; Popper, P. *Acta Crystallogr.* **1957**, *10*, 538; *ibid* **1958**, *11*, 54.
- (4) Pelloquin, D.; Hadermann, J.; Giot, M.; Caignaert, V.; Michel, C.; Hervieu, M.; Raveau, B. *Chem. Mater.* **2004**, *16*, 1715.

- (5) Dann, S. E.; Weller, T. M. *J. Solid State Chem.* **1995**, *115*, 499.

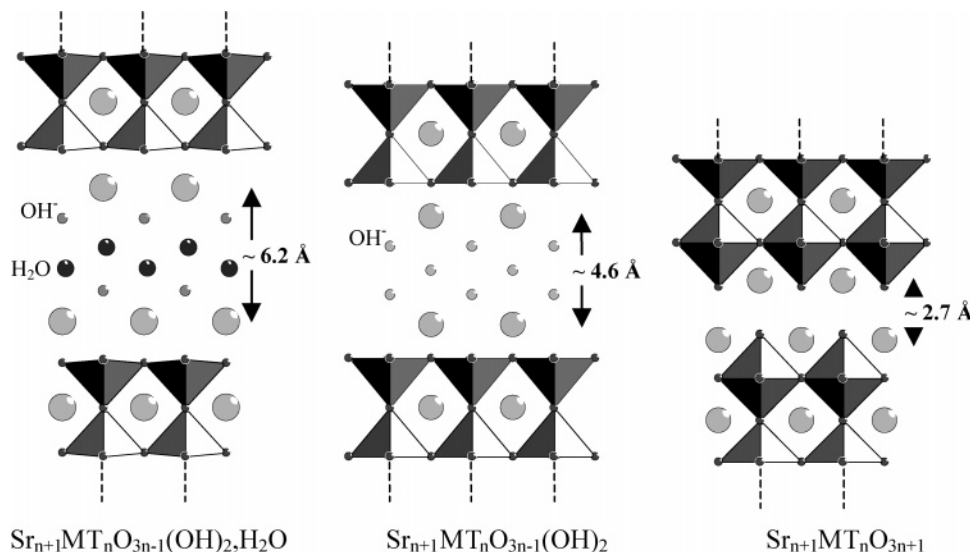


Figure 1. Left panel, hydrated oxyhydroxides $\text{Sr}_{n+1}\text{MT}_n\text{O}_{3n-1}(\text{OH})_2 \cdot \text{H}_2\text{O}$ (TM = transition metal) obtained by hydrolysis/hydration of the corresponding members of the RP series $\text{Sr}_{n+1}\text{MT}_n\text{O}_{3n+1}$ (right panel). By removing one H_2O molecule from the hydrated oxyhydroxide, the oxyhydroxides $\text{Sr}_{n+1}\text{MT}_n\text{O}_{3n-1}(\text{OH})_2$ are obtained. The thickness evolution depending to the intercalated groups of the block separating two successive perovskite blocks of n layers is given. The dashed lines are used to suggest the n layers.

The sample purity of these powders was checked by using X-ray powder diffraction patterns collected with a Philips X-pert Pro diffractometer ($\text{CuK}\alpha$ radiation). The latter is equipped with an Anton Paar TTK 450 chamber allowing the thermal decomposition in the range of 100–723 K to be reached under a nitrogen flow. The data were collected by step = 0.02° scanning over an angular range of $5^\circ \leq 2\theta \leq 80^\circ$, and the profile analysis of the diffraction peaks was performed with the JANA2000 program.⁶ The corresponding thermogravimetric analyses (TGA) were made with a SETARAM setup by the temperatures being varied up to 673 K under nitrogen flow.

The electron diffraction (ED) study was carried out using JEOL 200 CX transmission electron microscope (TEM) fitted with an eucentric goniometer ($\pm 60^\circ \text{C}$), whereas the high-resolution electron microscopy (HREM) images were recorded with a TOPCON 002B microscope operating at 200 kV and having a resolution point of 1.8 Å ($C_s = 0.4 \text{ mm}$). Both microscopes are equipped with KEVEX EDS analyzers.

The magnetic properties were measured by using a SQUID magnetometer and an ac susceptometer (extraction method), both systems from Quantum Design.

Results

Transmission Electron Microscope (TEM) Analyses. A first set of samples was prepared on the basis of a RP $n = 3$ member, by x being varied in $\text{Sr}_4\text{Co}_{3-x}\text{Ti}_x\text{O}_8$ from $x = 0$ to 1.5. The EDS analyses coupled to the electron diffraction study have revealed two distinct lattices, each corresponding to distinct cation compositions, $\text{Sr}_4\text{Co}_{1.6}\text{Ti}_{1.4}$ and $\text{Sr}_3\text{Co}_{1.7}\text{Ti}_{0.3}$, respectively. A second set of samples was then synthesized starting from these cation compositions.

The study by transmission electron microscopy of the latter confirms the great analogy with the RP structures. Thus, the $\text{Sr}_3\text{Co}_{1.7}\text{Ti}_{0.3}$ and $\text{Sr}_4\text{Co}_{1.6}\text{Ti}_{1.4}$ compounds, labeled in the following by $n = 2$ and 3, respectively, in reference to the RP series, exhibit in diffraction mode a monoclinic distorted

unit cell with $a \approx b \approx 3.8 \text{ Å}$ and $c \approx 28.2 \text{ Å}$ for $n = 2$ and $a \approx b \approx 3.8 \text{ Å}$ and $c \approx 35 \text{ Å}$ for $n = 3$, while the main reflection condition hkl , $h + k + l = 2n$, compatible with an I -type lattice, is the same for both samples. The extended stacking periodicity when compared to the RP titanates³, $c \approx 28 \text{ Å}$ instead of about 20 Å for $n = 2$ and $c \approx 35 \text{ Å}$ instead of 28 Å for $n = 3$, shows a large increase in the c parameter. The latter value, $c \approx 35 \text{ Å}$, is close to that reported for the iron based oxyhydroxide $\text{Sr}_3\text{NdFe}_3\text{O}_{7.5}(\text{OH})_2 \cdot \text{H}_2\text{O}$,⁴ whose structure is also related to the RP series. For this hydrated oxyhydroxide, the increase of the c stacking parameter from $c \approx 28$ to $c \approx 35 \text{ Å}$ is induced by the introduction of (OH^-) groups and water molecules at the level of the rocksalt-type layers. Taking into account the similarity between the ED patterns and X-ray diffraction pattern of the $n = 3$ sample, namely, $\text{Sr}_4\text{Co}_{1.6}\text{Ti}_{1.4}$, and those of the hydrated oxyhydroxide $\text{Sr}_3\text{NdFe}_3\text{O}_{7.5}(\text{OH})_2 \cdot \text{H}_2\text{O}$, a similar topotactic mechanism can be considered to explain the structures of these new layered (Co/Ti)-based materials.

The instability of the present samples under vacuum and electron beam of the TEM is consistent with such a hypothesis. Despite this sensitivity, illustrated by the diffuse spots on the $[100]$ ED patterns and the change of periodicity along the c axis after the irradiation under the electron beam as shown in Figure 2, an HREM study has been even so carried out to study the nature of the cation framework and the possible introduction of foreign groups. This work has been focused on the $n = 2$ sample, namely, $\text{Sr}_3\text{Co}_{1.7}\text{Ti}_{0.3}$. The two $[100]$ oriented images shown in Figure 3 have been recorded on the same crystal after an interval of several minutes. Clearly, the crystal matrix is affected under the electron beam as illustrated by the decrease of the periodicity along the stacking direction (white arrows in Figure 3b). For both images, the dark dots are correlated to the cation rows (defocus value close to -250 Å). They reveal five successive layers of dark dots, spaced at 3.8 Å along the b direction and shifted by 1.9 Å along the c axis. These contrasts are

(6) Petricek, V. et al. JANA 2000 software; Institute of Physics Academy of Science of the Czech Republic, Prague.

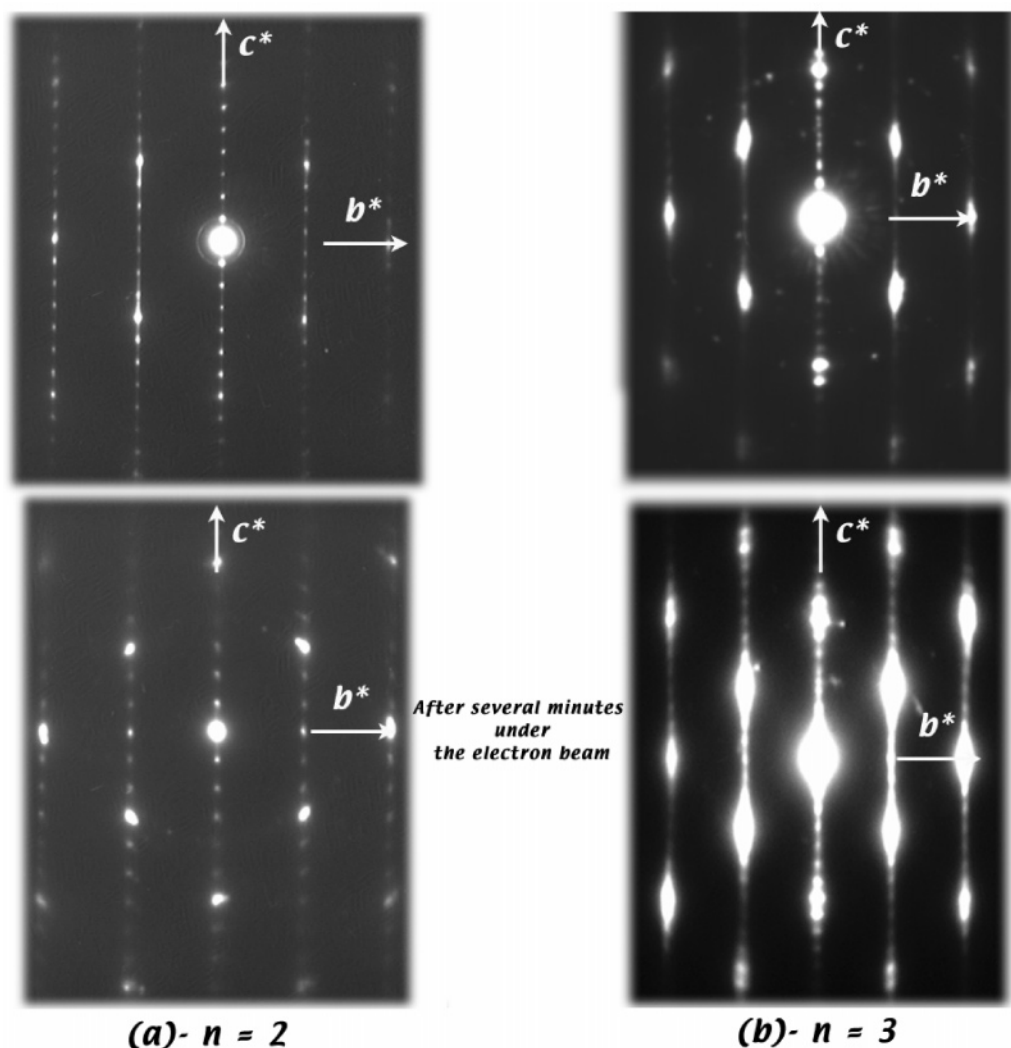


Figure 2. Experimental [100] oriented ED patterns recorded before and after a delay of several minutes under the electron beam for (a) $\text{Sr}_3\text{Co}_{1.7}\text{Ti}_{0.3}\text{O}_5(\text{OH})_{2,x}\text{H}_2\text{O}$ $n = 2$ and (b) $\text{Sr}_4\text{Co}_{1.6}\text{Ti}_{0.4}\text{O}_8(\text{OH})_{2,x}\text{H}_2\text{O}$ $n = 3$ compounds.

characteristic of a double perovskite and can be correlated to the sequence $[\text{SrO}]-[(\text{Co},\text{Ti})\text{O}_2]-[\text{SrO}]-[(\text{Co},\text{Ti})\text{O}_2]-[\text{SrO}]$. These blocks, 7.6 Å thick, are common to both images, and they differ only by the thickness of their separating layers. The initial image (Figure 3a) exhibits layers of lighter dots, 6.5 Å thick, whereas the second image (Figure 3b) exhibits various layers of similar contrasts but with various thicknesses, typically 4.5 or 6.5 Å. An enlarged zone along the edge of the crystal (Figure 4) allows us to detail these different light layers: the periodicity of about 6.5 Å results on zip-on quadruple layers, and in the middle of this block, a darker contrast of a varying thickness from 2.7 to 3.5 Å is observed (white arrows) along the b axis. The simultaneous loss of this intermediate specific layer and the related $\bar{b}/2$ translation lead to new contrasts as light crosses of about 4.5 Å thick. These specific contrasts can be compared to those observed in the case of the anhydrous $\text{Sr}_3\text{NdFe}_3\text{O}_{7.5}(\text{OH})_2$ oxyhydroxide,⁴ in which a similar decrease of about 2 Å of the stacking mode occurs during the structural change from hydrated oxyhydroxide to oxyhydroxide. These contrasts as light crosses would thus correspond to (OH^-) hydroxyl groups at the level of two theoretical $[\text{SrO}]^{\text{RS}}$ layers, which would be formulated $[\text{SrOH}]^{\text{RS}}$, separating the perovskite blocks. These peculiar layers would have the ability

to intercalate water molecules. Consequently, according to this structural evolution and to the analogy with the iron based hydrated hydroxide related to the $n = 3$ RP series, the theoretical formulas, $\text{Sr}_3\text{Co}_{1.7}\text{Ti}_{0.3}\text{O}_5(\text{OH})_{2,x}\text{H}_2\text{O}$ and $\text{Sr}_4\text{Co}_{1.6}\text{Ti}_{0.4}\text{O}_8(\text{OH})_{2,x}\text{H}_2\text{O}$ based on a hydration/hydrolysis mechanism and the EDS analyses, can be proposed for the compounds derived from $n = 2$ and 3 RP members, respectively.

Thermal Analyses. To validate these structural models, thermogravimetric and thermogravimetric analyses in N_2 flow have been made up to 450 °C. For both samples, the $[\text{mass}(T)/\text{mass}(T = 25\text{ °C})] = f(T)$ curve shows a clear tendency for this compound to lose weight as soon as it is warmed beyond 25 °C.

For the $n = 3$ phase, $\text{Sr}_4\text{Co}_{1.6}\text{Ti}_{0.4}\text{O}_8(\text{OH})_{2,x}\text{H}_2\text{O}$, a great analogy with the results obtained for $\text{Sr}_3\text{NdFe}_3\text{O}_{7.5}(\text{OH})_2$, H_2O compound⁴ is observed. Particularly, two major losses are observed at $T \approx 100\text{ °C}$ and then at $T \approx 300\text{ °C}$, while the total weight loss observed at 450 °C could correspond to the departure of approximately two water molecules (Figure 5). In parallel, the thermogravimetric analyses confirm the changes in the stacking periodicity as the temperature increases. The first structural transition, characterized by a decrease of the stacking periodicity from ≈ 18

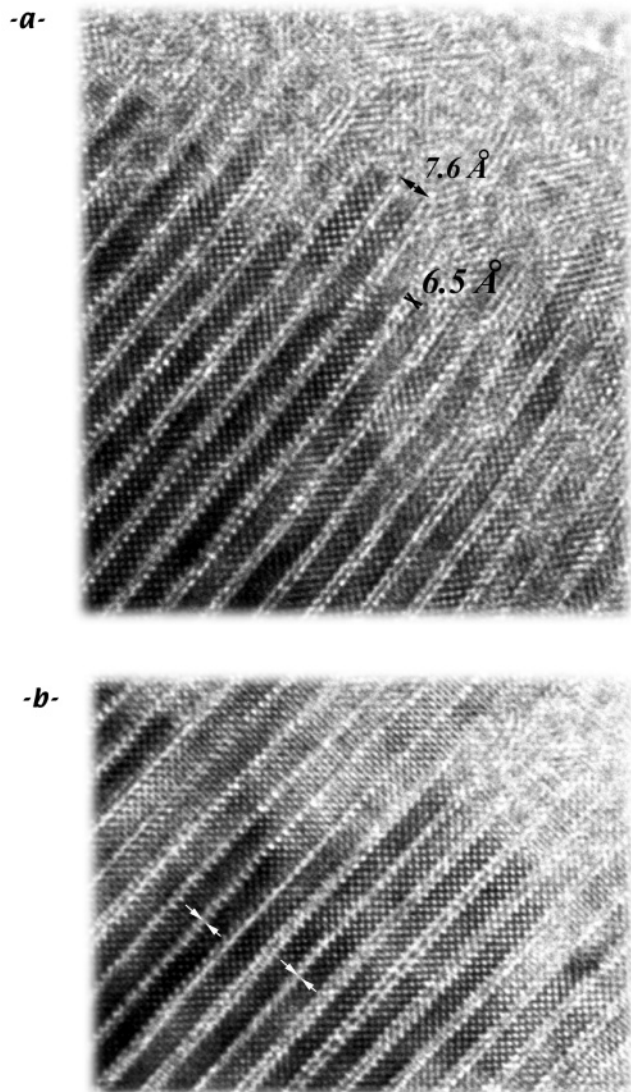


Figure 3. (a) Experimental [100] oriented HREM image recorded for $\text{Sr}_3\text{Co}_{1.7}\text{Ti}_{0.3}\text{O}_5(\text{OH})_2 \cdot x\text{H}_2\text{O}$ $n = 2$ compound with a defocus value Δf close to -250 Å. The same crystal recorded after several minutes under the electron beam is shown in panel b.

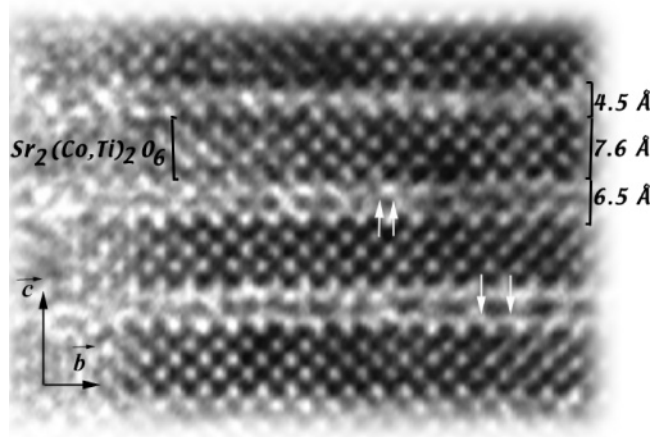


Figure 4. Enlarged [100] HREM image of the Figure 3b showing the occurrence of two distinct contrasts, thickness of 4.5 or 6.5 Å, between two double perovskite $\text{Sr}_2(\text{Co,Ti})_2\text{O}_6$ blocks.

to ≈ 16 Å, is associated to the departure of free water molecules as for the $\text{Sr}_3\text{NdFe}_3\text{O}_{7.5}(\text{OH})_2 \cdot \text{H}_2\text{O}$ compound.⁴ Thus, the second weight loss, around $T = 300$ °C, is

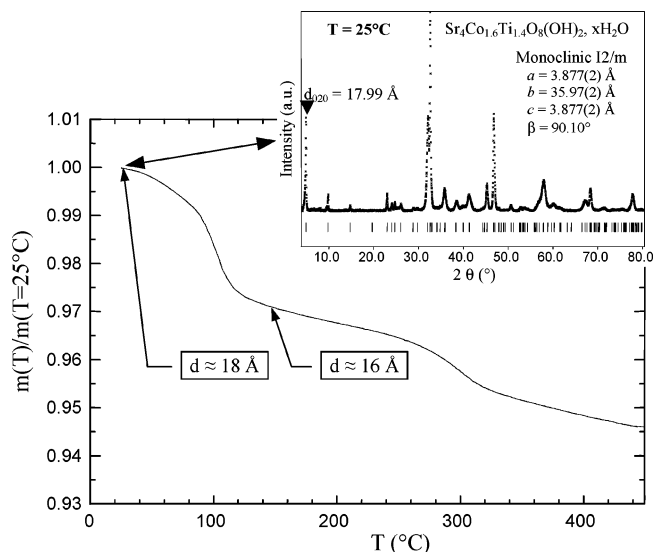


Figure 5. Thermogravimetric data of the hydrated hydroxide $\text{Sr}_4\text{Co}_{1.6}\text{Ti}_{1.4}\text{O}_8(\text{OH})_2 \cdot x\text{H}_2\text{O}$ $n = 3$ collected under nitrogen flow in the range from 25 to 450 °C and experimental XRD pattern collected at $T = 25$ °C. This pattern is indexed in the $12/m$ space group.

interpreted as the departure of the hydroxyl groups from $\text{Sr}_4\text{Co}_{1.6}\text{Ti}_{1.4}\text{O}_8(\text{OH})_2$ leading at $T = 400$ °C to an amorphous-like product.

In the case of the $n = 2$ phase, namely, $\text{Sr}_3\text{Co}_{1.7}\text{Ti}_{0.3}\text{O}_5(\text{OH})_2 \cdot x\text{H}_2\text{O}$, the evolution is more complex (Figure 6). The first part of the thermal decomposition is related to a dehydration mechanism starting from 60 °C. The weight loss is progressive and corresponds to about 2.5% as T reaches 200 °C. But for $T \geq 200$ °C, no plateau is really reached since a slight weight loss, of about 1%, occurs between 200 and 300 °C. Finally, a larger weight loss of about 4% occurs between 300 and 450 °C. The thermogravimetric analysis also reveals two gradual structural changes. At $T = 200$ °C, a first structural transition related to a decrease of the stacking periodicity from 14.1 to 12.7 Å and associated to the departure of free water molecules is indeed achieved. The final loss of the 12.7 Å periodicity related to the departure of hydroxyl groups is reached at $T = 450$ °C, while the decrease of the crystallinity of the compound is also observed.

In agreement with the topotactic features of this hydration/hydrolysis mechanism, if the warming is stopped at $T = 200$ °C, the change of the periodicity along the stacking axis observed for both $n = 2$ and $n = 3$ samples is found to be reversible. On the other hand, the oxyhydroxides formed at $T = 200$ °C and next cooled in air at room temperature return to their initial hydrated structural form.

Structural Refinements and Discussion. Despite the poor crystallization of these samples, structural refinements were made from the powder X-ray diffraction data to validate the RP-type framework deduced from TEM observations, and especially, to determine the thickness evolution of the block of layers separating the successive perovskite-type blocks. This work is focused on the $n = 2$ -type compounds, $\text{Sr}_3\text{Co}_{1.7}\text{Ti}_{0.3}\text{O}_5(\text{OH})_2 \cdot x\text{H}_2\text{O}$ and $\text{Sr}_3\text{Co}_{1.7}\text{Ti}_{0.3}\text{O}_5(\text{OH})_2$, respectively.

The X-ray pattern of $n = 2$ -type compound, $\text{Sr}_3\text{Co}_{1.7}\text{Ti}_{0.3}\text{O}_5(\text{OH})_2 \cdot x\text{H}_2\text{O}$, limited by the sample quality and the

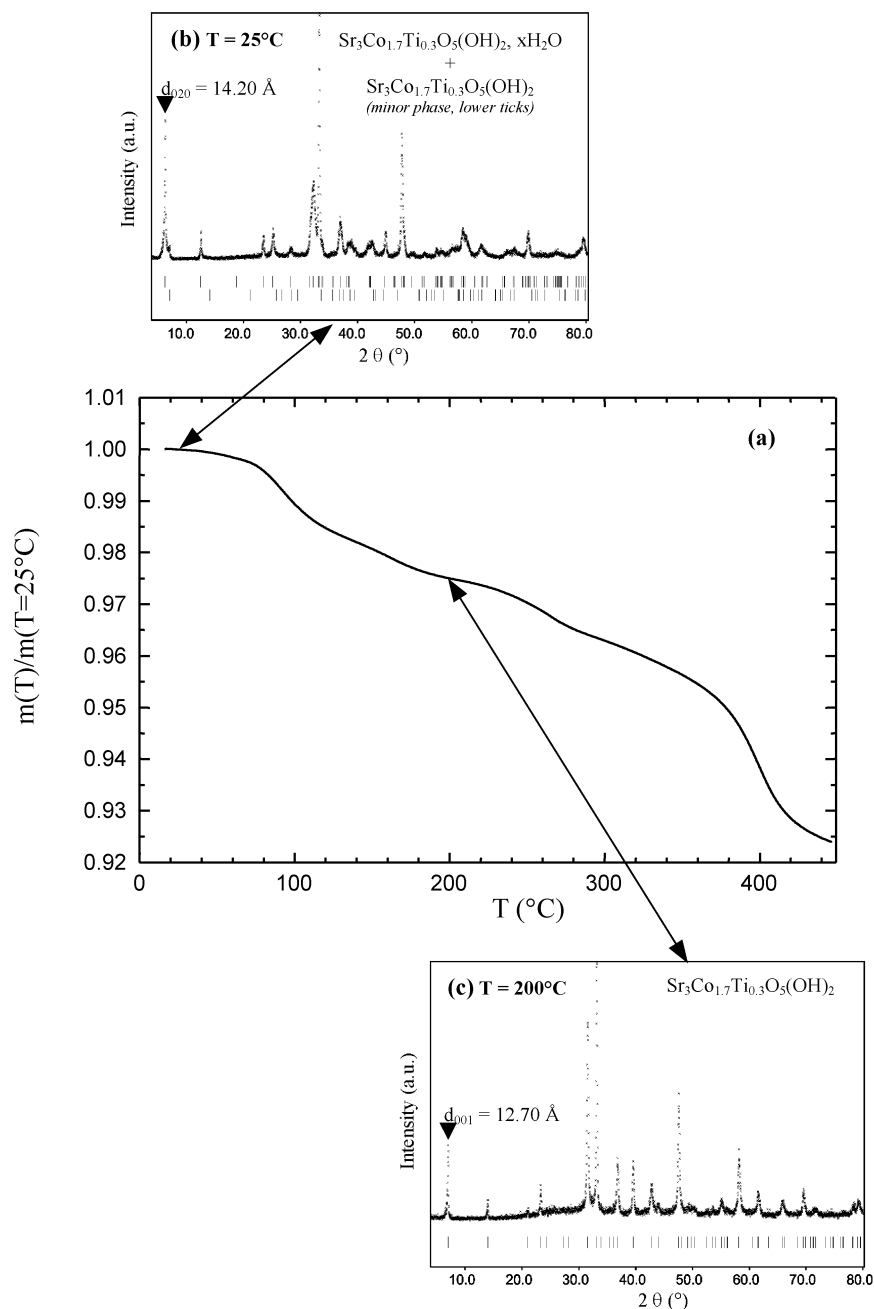


Figure 6. Thermogravimetric data of the hydrated hydroxide $\text{Sr}_3\text{Co}_{1.7}\text{Ti}_{0.3}\text{O}_5(\text{OH})_2 \cdot x\text{H}_2\text{O}$ $n = 2$ collected under nitrogen flow in the range from 25 to 450 $^\circ\text{C}$ and experimental XRD patterns collected at (a) $T = 25^\circ\text{C}$ and (b) $T = 200^\circ\text{C}$. Vertical bars are the Bragg angle positions corresponding to the space groups used (Table 1).

presence of the anhydrous form $\text{Sr}_3\text{Co}_{1.7}\text{Ti}_{0.3}\text{O}_5(\text{OH})_2$ as impurity, has been indexed by assuming a monoclinic unit cell with $a = c = 3.813(1) \text{ \AA}$, $b = 28.391(3) \text{ \AA}$, and $\beta = 90.3(1)^\circ$ ($I2/m$ space group). The observed intensities were extracted using the Jana2000 program (Le Bail method).⁶ From direct methods, using the SHELXS97 and EXPO programs,^{7–8} two Sr and one Co/Ti atomic sites are set in the structure, confirming the $n = 2$ RP-type stacking mode

for this compound. For Rietveld refinements, an initial model composed by the previous atomic positions and four other oxygen atom positions owing to the SrO and (Co/Ti)O₂ planes was introduced. At this stage of the refinement, the oxygen atom of the external SrO layer systematically moves toward the double-perovskite interlayer. In fact, Fourier difference maps show four significant electron residues between both successive SrO layers. Such an electron excess can be correlated to intercalated H₂O and OH[−] groups. The same process has been used to study the powder X-ray diffraction data recorded at $T = 200^\circ\text{C}$ (i.e., after the departure of about one H₂O molecule). The structure of the anhydrous $\text{Sr}_3\text{Co}_{1.7}\text{Ti}_{0.3}\text{O}_5(\text{OH})_2$ oxyhydroxide was solved in a tetragonal unit cell ($P4/mmm$ space group) with $a =$

(7) Sheldrick, G. M. *SHELX97—Programs for Crystal Structure Analysis (Release 97-2)*; Institut für Anorganische Chemie der Universität, Tammannstrasse 4, D-3400 Göttingen, Germany, 1998.

(8) Altomare, A.; Burla, M. C.; Camalli, M.; Carrozzini, B.; Cascarano, G.; Giacovazzo, C.; Guagliardi, A.; Moliterni, A. G. G.; Polidori, G.; Rizzi, R. EXPO: a program for full powder pattern decomposition and crystal structure solution. *J. Appl. Crystallogr.* **1998**, 32, 339.

Table 1. Crystallographic Parameters for $\text{Sr}_3\text{Co}_{1.7}\text{Ti}_{0.3}\text{O}_5(\text{OH})_{2-x}\text{H}_2\text{O}$ and $\text{Sr}_3\text{Co}_{1.7}\text{Ti}_{0.3}\text{O}_5(\text{OH})_2$

Sr ₃ Co _{1.7} Ti _{0.3} O ₅ (OH) _{2-x} H ₂ O					Sr ₃ Co _{1.7} Ti _{0.3} O ₅ (OH) ₂				
crystal system		monoclinic			crystal system		tetragonal		
space group		I12/m1 (no. 12)			space group		P4/mmm (no. 123)		
unit cell dimensions		a = 3.813(1) Å; b = 28.391(3) Å; β = 90.33(1)°; c = 3.813(1) Å			unit cell dimensions		a = 3.8263(7) Å; c = 12.700(3) Å		
cell volume		412.70(8) Å ³			cell volume		185.93(7) Å ³		
Z		2			Z		1		
peak shape		pseudo-Voigt			peak shape		pseudo-Voigt		
RF		0.109			RF		0.082		
Atomic coordinates									
atom	Wyck.	x	y	z	atom	Wyck.	x	y	z
Sr1	2d	0	0	−1/2	Sr1	1c	1/2	1/2	0
Sr2	4h	0	0.140(1)	−1/2	Sr2	2h	1/2	1/2	0.3027(5)
Co/Ti	4h	1/2	0.059(2)	0	Co/Ti	2g	0	0	0.1639(8)
O1	2c	1/2	0	0	O1	4i	0	1/2	0.181(2)
O2	4g	0	0.073(3)	0	O2	1a	0	0	0
O3	4g	1/2	0.079(3)	1/2	O ³ (OH-)	1d	1/2	1/2	1/2
O ⁴ (OH [−])	4h	0	0.233(3)	1/2	O ⁴ (OH-)	2g	0	0	−0.586(3)
O ₅ (H ₂ O)	4h	0	0.309(5)	1/2					

3.8263(7) Å and $c = 12.700(3)$ Å. Fourier syntheses from the atomic positions deduced by direct methods have allowed the localization of two extra atomic positions.

The structural models were then refined by the Rietveld method considering a common site for the Co/Ti species and fixing the ratio to the value found from the EDS analyses. Taking into account the bad crystallization of both structural forms, the refinements of occupancy sites and atomic displacements were not realistic, so the values given in the tables were arbitrarily fixed. The H₂O and OH⁻ groups have been modeled as extra oxygen atoms. Final values for the Bragg factors, $R_F = 0.109$ and 0.082 for the hydrated $\text{Sr}_3\text{Co}_{1.7}\text{Ti}_{0.3}\text{O}_5(\text{OH})_{2-x}\text{H}_2\text{O}$ and the anhydrous $\text{Sr}_3\text{Co}_{1.7}\text{Ti}_{0.3}\text{O}_5(\text{OH})_2$ hydroxide, respectively, are reasonable. The final structural parameters and corresponding structural drawings are shown in Table 1 and Figure 7.

For the starting hydrated oxyhydroxide compound, the thickness of the double perovskite layer and the interlayer block are 7.9 and 6.2 Å, respectively, in good agreement with the TEM results. The positions of the O4 and O5 sites in the interlayer must be carefully considered but could give a rough idea of the localization of the hydroxyl groups idealized by the O5 sites ($d_{\text{Sr1-O5}} = 2.63$ Å) and H₂O groups idealized by the O4 sites, respectively. In comparison with the room-temperature hydrated structure, the departure of water leading to the oxyhydroxide implies the loss of the *I* mode with the $(a + b)/2$ translation of the double perovskite block and a shortening of the stacking parameter from $c/2 = 14.15$ Å to $c = 12.69$ Å. The thickness of the perovskite-type blocks, 7.7 Å, is comparable to the previous one, 7.9 Å, but the interlayer distance decreased from 6.2 to 5.0 Å. In these separating blocks, the O4–O4 distance (2.26(5) Å) is too short for a fully occupied site. It is rather consistent with a half-filled site in agreement with the $\text{Sr}_3\text{Co}_{1.7}\text{Ti}_{0.3}\text{O}_5(\text{OH})_2$ formula. In this structure, the perovskite blocks are thus made of square pyramids instead of octahedra due to the presence of the hydroxyl groups in the interlayer. This structural feature is also reported in the case of the cobalt oxychlorides⁹ for which a 5-fold coordination was found for the cobalt. It must be emphasized that an accurate determination of the oxygen content is not made easy from redox

titrations since these samples are sensitive to moisture in a wet environment, and a very large uncertainty remains. Nonetheless, these hypothetical formulas $\text{Sr}_3\text{Co}_{1.7}\text{Ti}_{0.3}\text{O}_5(\text{OH})_{2-x}\text{H}_2\text{O}$ and $\text{Sr}_4\text{Co}_{1.6}\text{Ti}_{1.4}\text{O}_8(\text{OH})_{2-x}\text{H}_2\text{O}$ yield plausible cobalt oxidation states of ≈ 2.8 if one assumes that titanium cations are all tetravalent.

Magnetic Behavior. According to the structural changes induced by the loss of water at temperatures close to RT, the temperature dependent magnetic properties have been investigated in two stages. First, the magnetization (*M*) or magnetic susceptibility data (χ' , χ'') were collected by limiting the temperature to $T < 200$ K. In a second step, the data were finally collected up to 400 K. The compound derived from the $n = 3$ RP member, $\text{Sr}_4\text{Co}_{1.6}\text{Ti}_{1.4}\text{O}_8(\text{OH})_{2-x}\text{H}_2\text{O}$, exhibits very small χ' values with a very large temperature domain where the inverse susceptibility varies linearly with the temperature (Figure 8). An upturn deviation on the $\chi'^{-1}(T)$ curve is detected below ~ 25 K. Note that for this compound there is almost no χ change induced by a warming up to 400 K. The Curie–Weiss fitting of the linear part of the curve leads to $\theta_p \sim 0$ K, showing that no strong Co–O–Co magnetic interactions exist in this compound in agreement with the important dilution of the magnetic cobalt array induced by the $\sim 50\%$ Ti⁴⁺ (d^0) substitution for cobalt. Furthermore, the effective magnetic moment, $\mu_{\text{eff}} = 2.95\mu_B/\text{Co}$, indicates that the cobalt could be trivalent and have an intermediate spin ($S = 1$, $\mu_{\text{eff}}/\text{Co} \sim 2.8\mu_B/\text{Co}$). Nonetheless, the recent report of the high spin state for the Co³⁺ cations in a similar CoO₅ coordination in the layered $\text{Sr}_2\text{CoO}_3\text{Cl}_2$ oxychloride¹⁰ shows that this result must be interpreted very carefully, especially if one considers the remaining uncertainties in the structural refinements.

On one hand, this lack of long-range magnetic order, understood by considering the dilution of the Co–O–Co magnetic interactions created by the nonmagnetic Ti⁴⁺ cations, is consistent with a local disorder responsible for

- (9) Loureiro, S. M.; Felser, C.; Huang, Q.; Cava, R. J. *Chem. Mater.* **2000**, *12*, 3181.
- (10) Hu, Z.; Wu, H.; Haverkort, M. W.; Hsieh, H. H.; Lin, H. J.; Lorenz, T.; Baier, J.; Reichl, A.; Bonn, I.; Felser, C.; Tanaka, A.; Chen, C. T.; Tjeng, L. H. *Phys. Rev. Lett.*, in press.

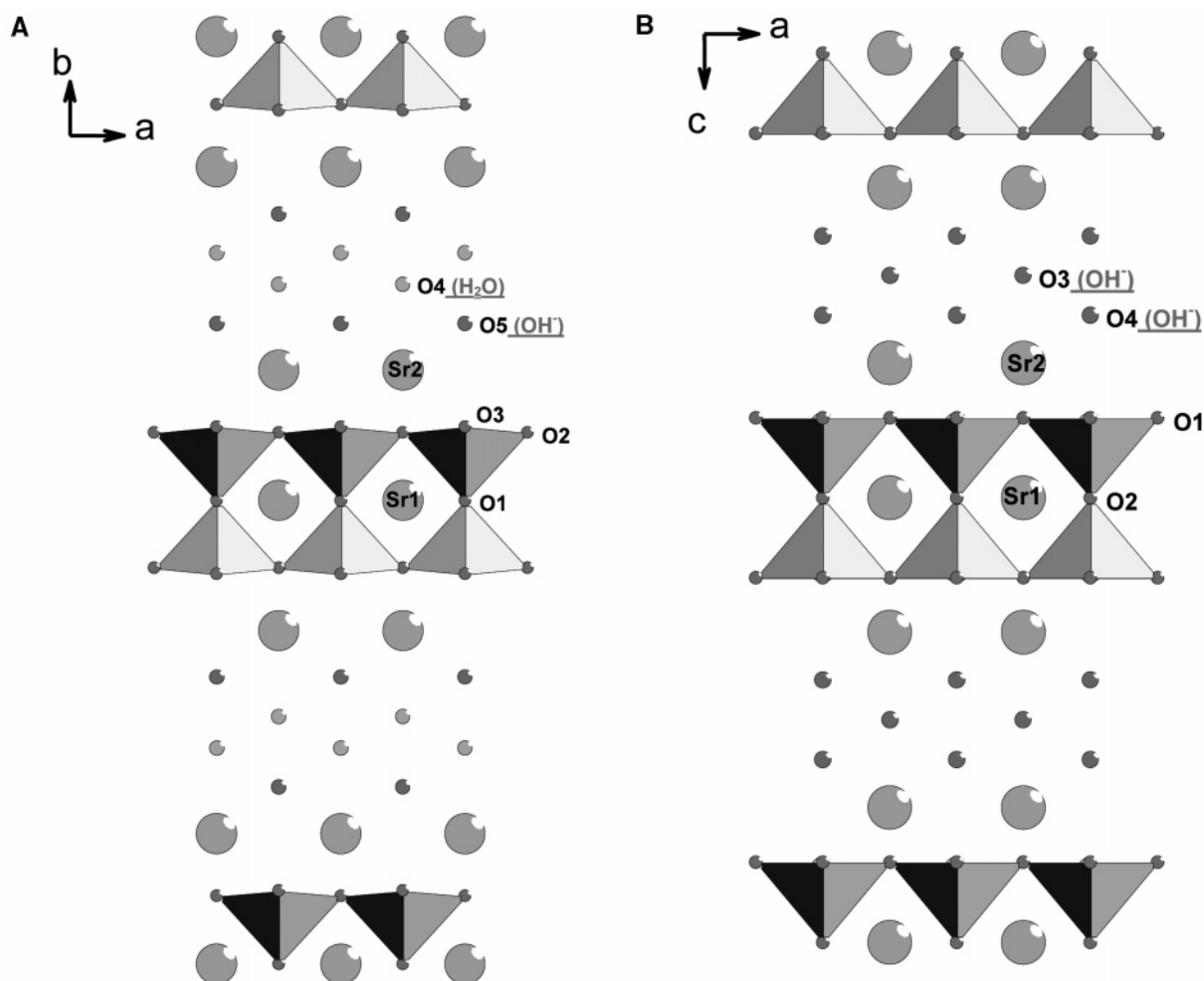


Figure 7. Structural models of (a) the $\text{Sr}_3\text{Co}_{1.7}\text{Ti}_{0.3}\text{O}_5(\text{OH})_2 \cdot x\text{H}_2\text{O}$ and (b) $\text{Sr}_3\text{Co}_{1.7}\text{Ti}_{0.3}\text{O}_5(\text{OH})_2$ $n = 2$ compounds.

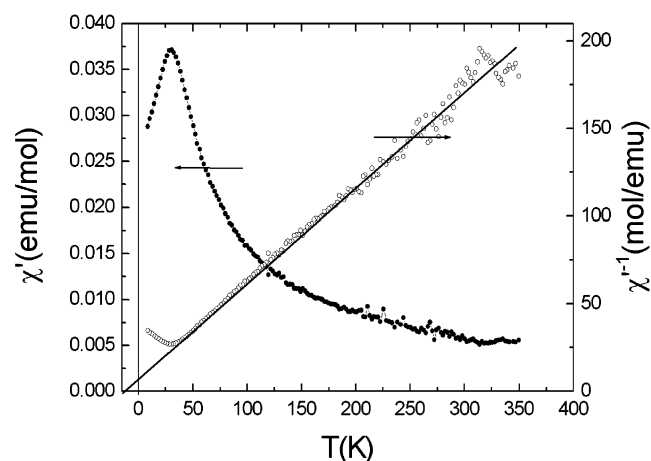


Figure 8. Temperature dependent ac magnetic susceptibility (real part χ') and corresponding $\chi'^{-1}(T)$ curve (right axis) for the $\text{Sr}_4\text{Co}_{1.6}\text{Ti}_{1.4}\text{O}_8-(\text{OH})_2 \cdot x\text{H}_2\text{O}$ $n = 3$ compound [$h_{\text{ac}} = 10$ Oe, $f = 10^4$ Hz]. The solid line on the $\chi'^{-1}(T)$ curve corresponds to the Curie-Weiss fitting.

magnetic frustrations between the positive and negative Co–O–Co magnetic exchange interactions. This is illustrated by the existence of a cusp on the $\chi'(T)$ curves (Figure 9), in which the temperature at the χ' maximum ($T_{\text{cusp}} \approx 30$ K) increases with the frequency (f) of the ac magnetic field. By assuming that this temperature corresponds to a spin freezing (T_f), one can calculate the K parameter, defined as $K = \Delta T_f / (T_f \Delta \ln f)$, often used to qualify the dynamics of a magnetic

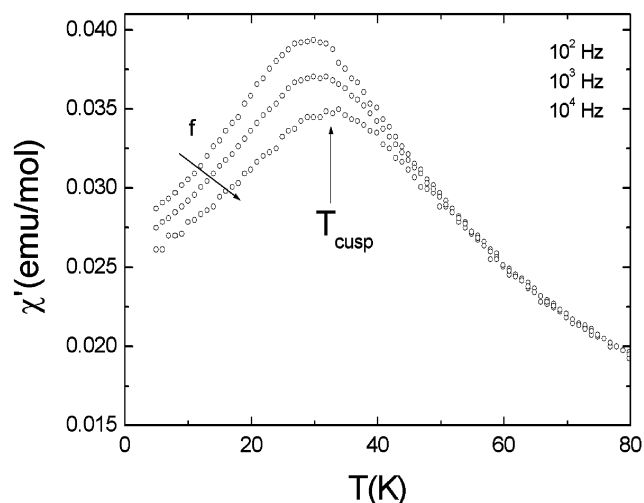


Figure 9. Enlargement of the $\chi'(T)$ curve of $\text{Sr}_4\text{Co}_{1.6}\text{Ti}_{1.4}\text{O}_8(\text{OH})_2 \cdot x\text{H}_2\text{O}$ $n = 3$ compound in the temperature region of the χ' maximum. The data are collected with $h_{\text{ac}} = 10$ Oe and for three different frequencies.

system.¹¹ One obtains $K = 0.09$ for $\text{Sr}_4\text{Co}_{1.6}\text{Ti}_{1.4}\text{O}_8-(\text{OH})_2 \cdot x\text{H}_2\text{O}$, a typical value for spin glasses.

In the case of the second hydrated oxyhydroxide $\text{Sr}_3\text{Co}_{1.7}\text{Ti}_{0.3}\text{O}_5(\text{OH})_2 \cdot x\text{H}_2\text{O}$, derived from an $n = 2$ RP member, the magnetic dilution by a nonmagnetic impurity is much less

(11) *Spin Glasses: an experimental introduction*; Mydosh, J. A., Ed.; Taylor and Francis: London and Washington, DC, 1993.

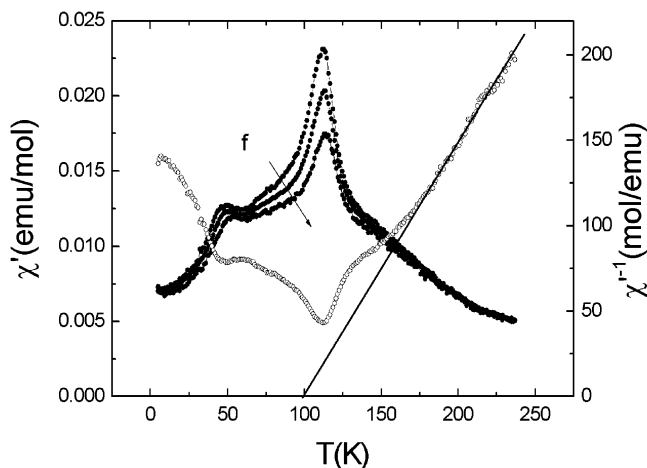


Figure 10. $\chi(T)$ (left axis) and $\chi^{-1}(T)$ (right axis) curve for the $\text{Sr}_3\text{Co}_{1.7}\text{Ti}_{0.3}\text{O}_5(\text{OH})_2 \cdot x\text{H}_2\text{O}$ $n = 2$ compound.

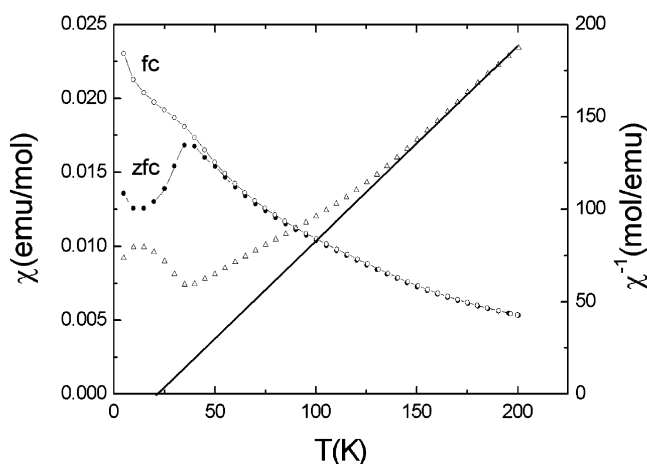


Figure 11. $\chi(T)$ curves obtained from magnetization measurements ($h_{dc} = 3 \times 10^3$ Oe) for the $\text{Sr}_3\text{Co}_{1.7}\text{Ti}_{0.3}\text{O}_5(\text{OH})_2 \cdot x\text{H}_2\text{O}$ $n = 2$ compound.

important (15% of cobalt site). As a result, the magnetism is much stronger as shown by the positive θ_p value, $\theta_p = 100$ K, obtained by extrapolating the $\chi^{-1}(T)$ curve to $\chi^{-1} = 0$ (Figure 10). This value must be compared to $\theta_p \approx 0$ K for the other member $\text{Sr}_4\text{Co}_{1.6}\text{Ti}_{1.4}\text{O}_8(\text{OH})_2 \cdot x\text{H}_2\text{O}$. Nonetheless, the magnetic behavior of this hydrated oxyhydroxide derived from an $n = 2$ RP member is much more complex than the other. The $\chi'(T)$ curve goes through a maximum value χ' at about 110 K with a very dramatic change of the χ' value as the h_{ac} frequency changes. Note also that χ' increases abruptly below about 125 K to reach this χ' maximum, suggesting also the appearance of a ferromagnetism in agreement with the $\theta_p > 0$ value. The existence of very large frequency effect could indicate the existence of a cluster-glass (i.e., small ferromagnetic islands grow below about 125 K, but their magnetic moments become frozen below about 110 K). This hypothesis is consistent with the shape of the $[M/H](T)$ curves, collected in zfc and fc modes (temperature maximum of 200 K) for a dc field of 0.3 T (Figure 11), which shows

only a slight inflection at 125 K better observed in the $\chi^{-1}(T)$ curve. For this large magnetic field value, the magnetization magnitude of the clusters is saturated so that the $\chi = M/H$ values are mainly governed by the magnetization of the paramagnetic matrix. On the other hand, the existence of a shoulder on the $\chi'(T)$ curve (Figure 10) and of an irreversibility between the zfc and fc curves (Figure 11) in the same temperature region, 30–40 K, shows that a spin-glass behavior also coexists in this sample. It must be emphasized that the occurrence of several changes of slope on the $\chi^{-1}(T)$ curves precludes the extraction of an unique μ_{eff} value. Finally, a shift in the $\chi^{-1}(T)$ curve location is observed before and after the sample is warmed to 400 K, which suggests that the cobalt magnetic states depend on the amount of foreign species (i.e., OH^- groups and H_2O molecules).

Conclusions

The present study shows that two new hydrated oxyhydroxydes $\text{Sr}_3\text{Co}_{1.7}\text{Ti}_{0.3}\text{O}_5(\text{OH})_2 \cdot x\text{H}_2\text{O}$ and $\text{Sr}_4\text{Co}_{1.6}\text{Ti}_{1.4}\text{O}_8(\text{OH})_2 \cdot x\text{H}_2\text{O}$, can be prepared in air. Their structural study by transmission electron microscopy and X-ray powder diffraction confirms that they both derive from RP $n = 2$ and 3 members. As previously shown in the isostructural iron-based oxyhydroxide hydrate, $\text{Sr}_3\text{NdFe}_3\text{O}_{7.5}(\text{OH})_2 \cdot \text{H}_2\text{O}$,⁴ water molecules can be inserted between two successive $[\text{SrOH}]^+$ layers. It must be pointed out that these structures differ from the oxide hydride, $\text{LaSrCoO}_3\text{H}_{0.7}$, in which hydride anion H^- is located at the level of the transition-metal layer.¹² From this viewpoint, the $[\text{SrOH}]^+$ layers are very similar to the $[\text{SrCl}]^+$ layers of the oxychlorides $\text{Sr}_3\text{Co}_2\text{O}_5\text{Cl}_2$.⁹ This is well-illustrated by the closeness of the stacking periodicity of $\text{Sr}_3\text{Co}_2\text{O}_5\text{Cl}_2$, $c/2 \approx 12$ Å, and that of the oxyhydroxide $\text{Sr}_3\text{Co}_{1.7}\text{Ti}_{0.3}\text{O}_5(\text{OH})_2$ observed at 200 °C, $c \approx 12.70$ Å. These compounds provide a new family of cobaltites in which the cobalt species adopt a square pyramidal coordination if one considers the long Co–OH apical distance. This distance, $d_{\text{Co–OH}} = 3.14$ Å is close to that reported for the oxychloride $\text{Sr}_3\text{Co}_2\text{O}_5\text{Cl}_2$ with $d_{\text{Co–Cl}} = 3.05$ – 3.30 Å.⁹

This chemical synthesis route provides a new opportunity to stabilize meta-stable phases by reaction of the high temperature stable phase with moisture while being cooled in air. Finally, the reversible character of the hydration must be also pointed out. By warming the hydrated oxyhydroxides to obtain the anhydrous oxyhydroxides $\text{Sr}_3\text{Co}_{1.7}\text{Ti}_{0.3}\text{O}_5(\text{OH})_2$ and $\text{Sr}_4\text{Co}_{1.6}\text{Ti}_{1.4}\text{O}_8(\text{OH})_2$, further exposition in air at room temperature allows the water molecules to be reintercalated at the level of the RS-type block to recover the hydrated oxyhydroxides.

CM048447K

- (12) Hayward, M. A.; Cussen, E. J.; Claridge, J. B.; Bieringer, M.; Rosseinsky, M. J.; Kiely, C. J.; Blundell, S. J.; Marshall, I. M.; Pratt, F. L. *Science* **2002**, 295, 1882.